High-resolution Beijing MST radar detection of tropopause structure and

variability over Xianghe (39.75° N, 116.96° E), China

Feilong Chen[1], Gang Chen[1*], Yufang Tian[2], Shaodong Zhang[1], Kaiming Huang[1],

Chen Wu[1], Weifan Zhang[1]

[1]School of Electronic Information, Wuhan University, Wuhan 430072, China.

[2]Key Laboratory of Middle Atmosphere and Global Environment Observation, Institute

of Atmospheric Physics, Chinese Academy of Sciences, Beijing 100029, China.

*Corresponding author: Gang Chen (g.chen@whu.edu.cn)

Abstract.

As a result of partial specular reflection from the atmospheric stable layer, the radar

tropopause (RT) can simply and directly be detected by VHF radars with vertical

incidence. Here, the Beijing MST radar measurements are used to investigate the

structure and the variabilities of the tropopause in Xianghe, China with a temporal

resolution of 0.5 hour from November 2011 to May 2017. High-resolution radar-

derived tropopause is compared with the thermal lapse-rate tropopause (LRT) that

defined by the World Meteorological Organization (WMO) criterion from twice daily

radiosonde soundings and with the dynamical potential vorticity tropopause (PVT) that

defined as the height of 2 PVU surface. During all the seasons, the RT and the LRT in

altitude agree well with each other with a correlation coefficient of ≥0.74. Statistically,

weaker (higher) tropopause sharpness seems to contribute to larger (smaller) difference

between the RT and the LRT in altitude. The RT agrees well with the PVT in altitude

during winter and spring with a correlation coefficient of ≥0.72, while the correlation

coefficient in summer is only 0.33. As expected, the monthly mean RT and LRT height both show seasonal variations. Lomb-Scargle periodograms show that the tropopause exhibits obvious diurnal variation throughout the seasons, whereas the semidiurnal oscillations are rare and occasionally observed during summer and later spring. Our study shows the good capability of the Beijing MST radar to determine the tropopause height, as well as present its diurnal oscillations.

Key words: VHF radar; MST radar; tropopause; diurnal oscillation.

1. Introduction

The tropopause marks a transition zone separating the well-mixed convectively active troposphere from the stably stratified and more quiescent stratosphere. Its structure and variability is characterized by large changes in thermal (e.g., lapse rate), dynamical (e.g., potential vorticity), and chemical properties (e.g., ozone and water vapor) and hence acts as a key role for the stratosphere-troposphere exchange (STE) processes (Hoinka, 1998; Seidel et l., 2001). The height of the tropopause depends significantly on the latitude, with about 17 km near the equator and less than 9-10 km at polar latitudes (Ramakrishnan, 1933). Over subtropical latitudes with the presence of subtropical jet, where the tropopause experiences rapid change or breaking, tropopause folding events are commonly observed (Pan et al., 2004). Climatologically, the altitude of the tropopause represents the seasonal variation of the flux of stratospheric air intruding into the troposphere (Appenzeller et al., 1996). Moreover, the tropopause height trends can be a sensitive indicator of anthropogenic climate

46   change (Sausen and Santer, 2003; Santer et al., 2003a; Añel et al., 2006).

47   A variety of ways are available to determine the extratropical tropopause.

48   Radiosonde sounding is the most commonly used to define the thermal tropopause

49   (hereafter referred to as LRT) based on temperature lapse-rate (WMO, 1957). The

50   thermal definition of tropopause can be applied globally and the tropopause height

51   easily be determined from one individual profile (Santer et al., 2003). Another feasible

52   definition is to use a specific potential vorticity (PV) surface to represent the dynamical

53   tropopause (hereafter referred to as PVT) (Reed, 1955; Hoskins et al., 1985).

54   Dynamical definition has the advantage that the PV is a conserved property (under

55   adiabatic and friction-less conditions) of an air mass (Hoskins et al., 1985; Bethan et

56   al., 1996). Values in the range 1-4 PVU (1 PVU= 10^6 m^2 s^{-1} K kg^{-1}) are used in

57   previous researches in the Northern Hemisphere (e.g. Baray et al., 2000; Sprenger et

58   al., 2003; Hoerling et al., 1991). The threshold of 2 PVU surface is the most commonly

59   used (Gettelman et al., 2011). Dynamical definition, however, is not applicable near the

60   equator, where the PV tends to be 0 (e.g., Hoerling et al., 1991; Nielsen-Gammon et al.,

61   2001). Creating a blended tropopause globally may probably a good way forward

62   (Wilcox et al., 2011). In addition, the data of GPS radio occultation satellites is also an

63   effective way and commonly applied to study tropopause (e.g. Schmidt et al., 2005;

64   Son et al., 2011).

65   As a result of partial specular reflection from stable atmospheric layer, the radar

66   tropopause (RT) can be well represented and identified by atmospheric radars operating

67   at meter wavelength (VHF band) and directing at vertical incidence (Gage and Green,

1979). Research activity increased remarkably following the first report on VHF radar

detection of tropopause by Gage and Green (1979), for instance, the researches in

middle latitudes (e.g. Hermawan et al., 1998), polar regions (e.g. Hall, 2013a), and

tropical regions (e.g. Das et al., 2008; Ravindrababu et al., 2014). Several methods have

been proposed to determine the tropopause height via radar echo power, including the

largest gradient in echo power (Vaughan et al., 1995; Alexander et al., 2013), the

maximum echo power (Vaughan et al., 1995; Hall et al., 2009), and the specific value

of echo power (Gage and Green, 1982; Yamamoto et al., 2003). The method of the RT

height determination used in this paper will be described in detail in next section.

The biggest advantage of the VHF radar measurements is the ability of continuous

operation unmanned in any weather conditions. Of course, no definition of the

tropopause is perfect. VHF radar system can only be limited to a few locations globally.

A detailed review of the close relationship between these different tropopause

definitions is provided by Alexander et al., (2012).

By means of the radiosonde, reanalysis, and satellite data available globally, long-

term (annual or longer) variability in tropopause height has received extensive attention

(e.g. Randel et al., 2000; Angell and Korshover, 2009; Son et al., 2011; Liu et al., 2014).

However, short period (diurnal or semidiurnal) variability of the tropopause is hard to

be examined by these measurements. In contrast, benefiting from the much higher

temporal resolution, radar definition of the tropopause provides good capability for

studying the diurnal and semidiurnal variation in tropopause height. Earlier, Yamamoto

et al., (2003) reported the capability of the Equatorial Atmospheric Radar to examine

90   the diurnal variation of tropopause height. Then, the diurnal variability of the tropical

91   tropopause was investigated in detail by Das et al., (2008) using the Indian Gadanki

92   MST radar. Its diurnal variation over a polar latitude station was investigated by Hall

93   (2013b). In the absence of pressure and temperature parameters, the evidence of

94   atmospheric tides can be well represented by winds (e.g. Huang et al., 2015).

95   The tropopause structure in midlatitudes is different from that in other regions.

96   Double tropopauses structure is a ubiquitous feature over mid-latitude regions near

97    $40°N$ (Pan et al., 2004; Randel et al., 2007). Strong evidence has revealed that the

98   poleward intrusion of subtropical tropospheric air that occurred above the subtropical

99   jet have resulted in the double structure (Pan et al., 2009). The higher part (second

100   tropopause near ~16 km) is characterized by tropical features of cold and higher level,

101   whereas the lower part (first tropopause near ~12 km) is characterized by polar features

102   of warm and lower level. In the present study, we focus only on the first tropopause

103   (below 16 km, if it exists) which will be referred to as 'tropopause' hereafter.

104   In this study, using more than 5 years of Beijing MST radar echo power

105   measurements in vertical beam, we mainly focus on the high-resolution characteristics

106   of the tropopause structure and their comparison with the simultaneous radiosonde and

107   dynamical definitions. Another important objective of this study is to examine the

108   diurnal and semidiurnal variability of the tropopause. The observational characteristics

109   of e.g. winds, echo power, and data acquisition rate near the tropopause layer are also

110   presented in the paper.

111

2. Data and Methods

2.1. Radar Dataset

As an important part of the Chinese Meridian Project, two MST radar systems are designed and constructed to improve the understanding of the extratropical troposphere, lower stratosphere, and mesosphere (Wang, 2010), which are Wuhan and Beijing MST radars. The Beijing MST radar located in Xianghe, Hebei Province, China (39.75° N, 116.96° E, 22 m above sea level) was designed and constructed by the Institute of Atmospheric Physics, Chinese Academy of Sciences and started its routine operation since 20 October 2011 (Tian and Lu, 2017). The radar is a high power coherent pulse-Doppler radar operating at 50 MHz with the maximum peak power of 172 kW and the half-power beam width of 3.2°. Five beams are applied: one vertically pointed beam and four 15° off-zenith beams tilted to north, east, south, and west. In order to obtain the high-quality measurements from troposphere, lower stratosphere, and mesosphere simultaneously, the radar is designed to operate routinely in three separate modes: low mode (designed range 2.5-~12 km), middle mode (10-~25 km), and high mode (60-~90 km) with vertical resolutions of 150, 600, and 1200 m, respectively. Under the routine operation, the 15-min break is followed by the 15-min operation cycle (5 min for each mode). As a result, the time resolutions of the low, middle, and high mode measurements are all 30 min. More detailed review of the radar system is given by Chen et al. (2016).

Here only the low mode echo power measurements are used to determine the RT height. Although the designed detectable range of the low mode is from 2.5-~12 km,

134 the vertically pointed beam can receive stronger echoes from a higher level (~14-15 km)

135 as compared with those from off-vertical beams due to the partial specular reflection

136 mechanism. The measurements in middle mode are also applied to calculate the winds

137 or echo power within ~5-6 km of the tropopause. The parameters for the two routine

138 operation modes are listed in Table 1. The monthly total number of the echo power

139 profiles available in vertical beam (low mode) is shown in Fig. 1. The outliers or

140 severely contaminated data that mainly induced by system problems are eliminated.

141 The large data gap in September is due to the annual preventive maintenance.

142 **2.2. Tropopause Definitions**

143 Due to the large gradient in potential temperature, radar return power received at

144 vertical incidence is significantly enhanced upon the transition zone of the tropopause

145 layer. Using this characteristic, the RT height can be determined effectively by the VHF

146 radar. Here, the RT is defined as the altitude (above 500 hPa) where the maximum

147 vertical gradient of echo power is located (Vaughan et al., 1995; Alexander et al.,

148 2013; Ravindrababu et al., 2014; Chen et al., 2018). Considering the occasional and

149 random noise, to which the derived-RT is sensitive, the echo power profiles are

150 smoothed by a 3-point running mean. In order to further reduce the influence of the

151 noise, the RT definition used here need to satisfy an additional criterion: the determined

152 RT height should be continuous with the adjacent RT heights (one on each side),

153 otherwise to search for the second peak gradient (eliminated if the second peak does

154 not meet the additional criterion). The "continuous" here means that the discrepancy

155 between the two successive heights (in time, 0.5-hour interval) should be <0.6 km. A

7

156   typical example of the RT and LRT is illustrated in Fig. 2. The LRT is identified based

157   on the World Meteorological Organization (WMO) criteria (WMO, 1957). The radar

158   aspect sensitivity is expressed as the ratio between vertical (p_v) and oblique (p_o) beam

159   echo power (here is 15° east beam). The radiosonde soundings are launched twice daily

160   from the Beijing Meteorological Observatory (39.93 ºN, 116.28 ºE, station number

161   54511), which is less than 45 km to the radar site. In this case, the LRT and RT

162   consistent well and are at 11.65 km and 11.85 km respectively. As expected, the LRT

163   characterized by a rapid increase in potential temperature gradient also corresponds to

164   the large gradient in radar aspect sensitivity. Note that the height with maximum value

165   in echo power lie at a higher altitude (as compared with the RT height) of ~700 m above

166   the LRT. The dynamical tropopauses used in this paper are derived from the European

167   Centre for Medium-Range Weather Forecasts (ECMWF) ERA-Interim Reanalysis (Dee

168   et al., 2011) and defined as the surface of 2 PVU potential vorticity, which is same to

169   that used by Sprenger et al., (2003) and Alexander et al. (2013).

170   **2.3. Tropopause sharpness definition**

171   For the compared data pairs between the RT and LRT, we calculate the

172   corresponding tropopause sharpness that represents the strength of the tropopause

173   inversion layer. As defined by Wirth, (2000), the tropopause sharpness S_{TP} can be

174   calculated as:

175    $$S_{TP} = \frac{T_{TP+\Delta z} - T_{TP}}{\Delta z} - \frac{T_{TP} - T_{TP-\Delta z}}{\Delta z} \tag{1}$$

where TP denotes the tropopause height, $\Delta z = 1$ km, and T_{TP} indicates the corresponding temperature. This definition is also used in Alexander et al. 2013 and we're using it for a good comparison with our results.

3. Results

3.1. High-resolution radar tropopause structure

The fine-scale height-time cross section of radar echo power and aspect sensitivity is shown in Fig. 3 for a typical month (February 2014), along with the RT, PVT and LRT marked in the figure. In general, the RT agreed well with both the LRT and PVT in height, and most of the RT exhibit a slightly higher altitude. However, the differences between the RT and LRT are sometimes large (reach to ~1-2 km) especially when the RT experience rapid change. Regardless of the background synoptic condition, the difference in the definitions themselves is to a large degree the main contributing factor for the large difference between the RT and LRT. For example, a second layer with significant enhanced echo power is observed above the radar-derived RT for the cases on 4 and 5 February 2012 (Fig.3a). According to the definitions, the RT well defined as the first layer with echo enhanced and the LRT matched the second layer, similar to that observed by Yamamoto et al., (2003) and Fukao et al., (2003). It is of note that the RT well separates the troposphere characterized by low aspect sensitivity from the lower-stratosphere characterized by high aspect sensitivity (Fig.3b).

3.2. Comparisons between different definitions

To further quantify the consistency and difference in altitude between different tropopause definitions, a detailed comparison is carried out in this section. The seasonal

198 scatterplots for RT versus LRT and the histogram distribution of altitude differences

199 between the RT and LRT are illustrated in Fig. 4, during the period November 2011-

200 May 2017. A total of 2411 data pairs are obtained for comparison. Among them, the

201 number of data pairs is 845 for DJF (winter), 721 for MAM (spring), 321 for JJA

202 (summer), and 524 for SON (autumn). Comparisons have shown a good consistency

203 throughout the seasons and most of the RTs exhibit a slightly higher than the LRTs. The

204 correlation coefficient is 0.74, 0.80, 0.82, and 0.78 for DJF, MAM, JJA, and SON,

205 respectively. The mean and standard deviation difference (RT minus LRT) calculated

206 in DJF, MAM, JJA, and SON is (0.14 ± 0.75), (0.26 ± 0.78), (0.33 ± 0.56), and

207 (0.12 ± 0.69) km, respectively. The proportion of the data pairs with differences <500 m

208 is reasonably good during four seasons and is 63%, 61%, 64%, and 67% for DJF, MAM,

209 JJA, and SON, respectively. Fig. 4 explicitly shows that the RT derived by the Beijing

210 MST radar agrees reasonably well with the LRT throughout the seasons.

211   To examine the potential role of the sharpness, Fig. 5a and Fig. 5b show the

212 histogram distribution of the tropopause sharpness along with the probability density

213 curve for data pairs with difference (absolute values of RT minus LRT) <0.5 km and >1

214 km respectively. What is apparent is that most data pairs of Fig. 5a are located to the

215 right (higher sharpness values, with the peak of ~7.06 K/km) and of Fig. 5b are to the

216 left (lower sharpness values, with the peak of ~6.35 K/km). No matter whether this

217 distribution feature is associated with the cyclonic-anticyclonic systems (e.g. Randel et

218 al., 2007; Randel and Wu, 2010), the results more or less demonstrate that the larger

219 (weaker) tropopause sharpness contribute to lower (higher) difference between the RT

220 and LRT. From the perspective of seasonal statistics, the tropopause sharpness over

221 Beijing station shows similar distribution characteristics throughout the seasons (not

222 shown), which is different from that in polar regions where the sharpness is significantly

223 higher during summer than during winter (Zängl and Hoinka, 2001).

224   The seasonal scatterplots and height difference distribution between the RT and

225 PVT are illustrated and quantified in Fig. 6. The total number of comparing data pairs

226 for winter, spring, summer, and autumn is 1422, 1260, 791, and 1145, respectively.

227 During winter and spring (Fig. 6a and 6b), the RTs agree reasonably well with the PVTs

228 with the correlation coefficient of 0.72 and 0.76 and the mean difference (RT minus

229 PVT) of (0.55±0.84 km) and (1±0.89 km), respectively. In contrast, the consistency

230 for summer and autumn (Fig. 6c and 6d) is relatively bad and with correlation

231 coefficient of 0.33 and 0.47 and mean difference of (0.80±1.39 km) and (0.75±1.23

232 km), respectively. Especially for summer, the proportion of the comparing data pairs

233 with difference <0.5 km is only 10.6% (84). In autumn, need to note that most data pairs

234 with poor consistency is sampled during early autumn.

235 **3.3. Observational characteristics in the vicinity of tropopause**

236   Measurements of radar middle mode are used for examining the horizontal wind,

237 return power, and effective wind data acquisition rate within 5-6 km of the tropopause

238 (upper troposphere and lower stratosphere). Left panels of Fig. 7 show the vertical

239 scatterplots of the static stability (represented by the buoyancy frequency squared) as a

240 function of height relative to the LRT and the right panels show the radar echo power

241 as a function of height relative to the RT, during two specific years 2012-2013 for

242   extended winter NDJFM and summer MJJAS seasons. Mean and standard deviations

243   are also plotted in each panel of Fig. 7. As expected, results clearly show sudden jump

244   in static stability and radar power near the tropopause layer. The degree of sudden

245   increase in echo power is more gradual than that in static stability. The amplitude of the

246   sudden increase in radar power experienced a slightly larger during NDJFM than that

247   during MJJAS (red lines of right panels). Another interesting feature in the lower-

248   stratosphere is that both the static stability and radar power points show less disperse

249   during NDJFM than that during MJJAS.

250   Fig. 8 shows the profiles of mean radar effective wind data acquisition rate for low

251   and middle modes during November 2011-May 2017. Clearly, both profiles exhibit a

252   sudden increase with height near the tropopause, with the first peak located ~1 km

253   higher above the mean tropopause height. Note that the second inversion in middle

254   mode profile that occurred near 16 km is associated with the second tropopause. As

255   limited by the highest detectable altitude (the data acquisition rate decreased to lower

256   than 20% at ~16 km), the profile in low mode shows little evidence of second inversion.

257   Fig. 9 shows time-height intensity plot of the monthly mean radar-derived

258   horizontal wind (from middle mode) during November 2011-May 2017, together with

259   the monthly mean location of RT and LRT. One pixel grid denotes 1 month×0.6 km.

260   The monthly mean RT and LRT agreed well with each other in height, within 400 m in

261   August and September and even lower in other months of about within 200 m. They

262   both exhibit a clear seasonal variation, with maximum in early autumn of ~11.6 km and

263   minimum in early spring of ~10.3 km. The monthly mean wind jet varies with season,

264   with the thinnest thickness and lowest strength in summer. The mean tropopause height

265   appears to correspond to the lower boundary location of peak wind layer. The error bars

266   of both the RT and LRT help to illustrate that the tropopauses changes by larger

267   amplitude in winter and June than that in other months.

268   **3.4. Periodogram analysis of the radar tropopause**

269   High temporal resolution detection of tropopause by VHF radar have allowed us

270   to investigate the diurnal or semidiurnal variability of the tropopause. Atmospheric tides

271   are well known global oscillations contributing to the diurnal variation in temperature

272   and background winds, which in turn modulate the tropopause height. With the absence

273   of high resolution temperature measurements, radar-derived winds are combined used

274   to represent the evidence of diurnal or semidiurnal variation in tropopause height that

275   modulated by tidal. The frequency power spectrum of the RT height, zonal and

276   meridional wind, calculated by means of Lomb-Scargle method (Press and Rybicki,

277   1989), is illustrated in Fig. 10 for two typical months: May 2015 and December 2016.

278   The choice of Lomb-Scargle algorithm is due to the presence of data gaps (~2 days per

279   week, especially during 2012-2013). The dominant ~24 h periodicity in RT height,

280   zonal and meridional wind is obvious for both months. The evidence of ~12 h period in

281   all three parameters is distinct for May 2015 (Fig. 10a), although the power is relatively

282   weaker. Through the analysis for each individual month, we found that the semidiurnal

283   component in the three parameters is generally and occasionally observed in summer

284   and later spring during our experimental period. The characteristics of the diurnal

285   variation of the RT height can be represented better in Fig. 11, which shows the mean

286   Lomb-Scargle power spectrum of the RT as a function month during November 2011-

287   May 2017. As compared with other months, the dominant diurnal periodicity is less

288   evident in April. We need to clarify that atmospheric tides are of course not the only

289   source of the diurnal variation in tropopause height, diurnal convective activities

290   (Yamamoto et al., 2003) might also be an important cause. Here will not be detailly

291   discussed.

292

293   **4.   Discussion**

294   As for the radar echo power definition, the RT estimation sometimes will fail due

295   to the system problems, even if the thermal tropopause is well defined (Hall et al., 2009).

296   Apart from the system problems, the following two conditions are primarily responsible

297   for the failure (or difficulty) of both the radar and thermal definitions over the radar site

298   latitude (~40° N). Firstly, the temperature sometimes continue to decrease upon into the

299   lower stratosphere (below 16 km) in summer and early autumn, leading to the

300   failure/difficulty of both the radar and thermal definitions (a typical case as shown in

301   Fig. 12a). Need to note that the temperature inversion layer occurred at ~16 km in

302   summer or early autumn is the second tropopause with characteristics of Tropics (Pan

303   et al., 2004; Randel et al., 2007). Secondly, some specific meteorological processes can

304   lead to the ambiguities and indefiniteness in thermal and radar definitions, such as

305   fronts, cyclones or typhoons, and folding (e.g. Nastrom et al., 1989; May et al., 1991;

306   Roettger, 2001; Alexander et al., 2013). Such ambiguities often result in large difference

307   in altitude between the RT and LRT. In addition, when multiple temperature inversion

14

308 layers occurred (below 16 km), the RT generally matched the lower part and LRT often

309 matched the upper part (e.g. Yamamoto et al., 2003; Fukao et al., 2003), such as the

310 double layers of enhanced echo power shown in Fig. 3 on 4 and 5 February 2012. Apart

311 from the two situations above, there is another condition that is commonly responsible

312 for the failure of thermal definition in summer and early autumn. As the typical case

313 shown in Fig. 12b, a significant inversion in temperature (at ~12 km) is recorded from

314 the radiosonde profile, but this inversion layer is too thin and weak to meet the WMO

315 criterion that thermal definition required. Whereas, the apparent enhancement in radar

316 echo power corresponding to such inversion layer is strong enough to well define the

317 RT. Need to highlight again that the temperature inversion located near ~16 km (the

318 second tropopause) is not the focus of this paper.

319   Pan et al., (2004) have reported that the difference between the LRT and PVT are

320 more distinct in the vicinity of subtropical jet. In the northern hemisphere, the axis of

321 the subtropical jet is situated near ~30°N in spring and winter, whereas in summer and

322 early autumn the subtropical jet shifts northward to ~40°N (see Fig. 4 in Ding and Wang,

323 2006). We preliminary considered that the bad consistency between the RT and PVT in

324 summer and early autumn (Fig. 6c and 6d) is most likely associated with the subtropical

325 jet shifting poleward to ~40°N. The existing cyclones or anticyclones in the upper-

326 troposphere (Wirth, 2000), of course, may also be an important influence factor for the

327 significant asymmetric differences (most of the scattered points deviate significantly

328 from the 1:1 line). The asymmetric differences, that is most of the RT are located higher

329 than the 2PVU tropopause height, suggest that the 2PVU surface is not the best measure

of a dynamical tropopause over Beijing during summer-time. More detailed discussion

about the striking asymmetric differences in height between LRT and PVT can be seen

in Wirth (2001) and will not be given here. Anyway, we need to be careful when using

the 2PVU dynamical definition to define the tropopause over radar site latitude ~40° N,

especially in summer.

About the characteristics of tropopause and the comparison between different

definitions, there are many differences between mid-latitude and polar regions. In mid-

latitude (~40°N), our results show that: (1) the agreement between RT and LRT is

similar good throughout the seasons; (2) RTs are generally located higher than the LRT;

(3) the thermal definition sometimes fail in summer and early autumn; (4) the

agreement between the RT/LRT and PVT in summer is poor. Whereas, in contrast,

previous researches about the tropopause over polar regions showed that (Wirth, 2000；

Alexander et al., 2013): (1) the difference between the RT and LRT is larger during

winter than that during summer; (2) RTs are generally located lower than the LRT; (3)

the thermal definition sometimes fail in winter and spring; (4) comparison between the

RT and PVT showed the similar good agreement during both summer and winter.

Over a polar latitude station, the seasonal characteristics of the diurnal oscillation

in tropopause height were investigated using 5 years of SOUSY VHF radar

measurements (Hall, 2013b). The sunlight variability in polar regions is different from

that in other latitudes of the world. Different sunlight variation actually will lead to

difference in atmospheric tides, and then would result in different diurnal variation in

tropopause height. Here we found that the diurnal oscillation of RT height at Xianghe

is ubiquitous and obvious throughout the seasons except for April (Fig. 11). Whereas at

polar latitude and in months of November to February when there is no sunlight, Hall

(2013b) observed little evidence of 24 h diurnal variability in RT height.

5. Conclusions

In this paper, we present the high resolution structure and variability of the

tropopause in Xianghe, China (39.75° N, 116.96° E), based on the Beijing MST radar

vertical beam echo power data collected during the period November 2011-May 2017.

Fine-scale structure of the RT is well determined with a high temporal resolution of 0.5

h. Comparison results have shown good agreement in altitude between the RT and LRT,

with a correlation coefficient of ≥ 0.74 for the four seasons. Higher tropopause

sharpness seems to contribute lower difference between the RT and LRT in altitude and

weaker sharpness appears responsible for higher difference. The agreement between

the RT and PVT is relatively well in winter and spring with correlation coefficient of

0.72 and 0.76 respectively, but poor during summer with a correlation coefficient of

only 0.33. We initially suggested that the poor consistency between RT and PVT is

associated with the subtropical jet shifting poleward to ~40°N.

As expected, the sudden jump in static stability (represented by the buoyancy

frequency squared) and the rapid increase in radar echo power upon the tropopause

layer are clearly observed. Upon the tropopause layer, a sudden increase in effective

radar data acquisition rate is also observed. Both the monthly mean RT and LRT height

have shown a clear annual cycle. The variability and oscillation of RT height with

diurnal or lower timescales is presented. Obvious diurnal variation in tropopause height, zonal wind, and meridional wind is generally observed throughout the seasons, indicating the modulation most likely from the atmospheric tides. The semidiurnal variation in RT height is not so obvious and commonly observed occasionally in summer and late spring.

References

Alexander, S.P., Murphy, D.J., and Klekociuk, A.R.: High resolution VHF radar measurements of tropopause structure and variability at Davis, Antarctica (69◦ S, 78◦ E), Atmos. Chem. Phys., 13, 3121-3132, 2013.

Angell, J. K., and Korshover, J.: Quasi-biennial and long-term fluctuations in tropopause pressure and temperature, and the relation to stratospheric water vapor content. Monthly Weather Review, 102(1), 29-34, 2009.

396 Appenzeller, C., Holton, J. R., and Rosenlof, K. H.: Seasonal Variation of Mass

397   Transport Across the Tropopause. Journal of Geophysical Research, 101(D10),

398   15071-15078, 1996.

399 Añel, J. A., J. C. Antuña, L. de la Torre, R. Nieto, and Gimeno L.: Changes in

400   tropopause height for the Eurasian region determined from CARDS radiosonde

401   data. Naturwissenschafte, 93, 603–609, doi:10.1007/s00114-006-0147-5, 2006.

402 Bethan, S., Vaughan, G., and Reid, S. J.: A comparison of ozone and thermal tropopause

403   heights and the impact of tropopause definition on quantifying the ozone content

404   of the troposphere. Quarterly Journal of the Royal Meteorological Society,

405   122(532), 929-944, 1996.

406 Baray, J., Daniel, V., Ancellet, G., and Legras, B.: Planetary-scale tropopause folds in

407   the southern subtropics. Geophysical Research Letters, 27(3), 353-356, 2000.

408 Chen, F. L., Chen, G., Shi, C. H., Tian, Y. F., Zhang, S. D., and Huang, K. M.: Strong

409   downdrafts preceding rapid tropopause ascent and their potential to identify cross-

410   tropopause stratospheric intrusions, Annales Geophysicae, 36(5), 1403-1417,

411   2018.

412 Chen, G., Cui, X., Chen, F., Zhao, Z., Wang, Y., Yao, Q., and Gong, W.: MST Radars

413   of Chinese Meridian Project: System Description and Atmospheric Wind

414   Measurement. IEEE Transactions on Geoscience and Remote Sensing, 54(8),

415   4513-4523, 2016.

416   Das, S. S., Jain, A. R., Kumar, K. K., and Rao, D. N.: Diurnal variability of the tropical

417   tropopause: Significance of VHF radar measurements. Radio Science, 43(6), 1-14,

418   doi:10.1029/2008RS003824, 2008.

419   Dee, D. P., Uppala, S. M., Simmons, A. J., Berrisford, P., Poli, P., Kobayashi, S. et al.:

420   The ERA-Interim reanalysis: configuration and performance of the data

421   assimilation system. Quarterly Journal of the Royal Meteorological Society,

422   137(656), 553-597, 2011.

423   Ding, A., and Wang, T.: Influence of stratosphere-to-troposphere exchange on the

424   seasonal cycle of surface ozone at Mount Waliguan in western China. Geophysical

425   Research Letters, 33(3), 233-252, doi:10.1029/ 2005GL024760, 2006.

426   Fukao, S., H. Hashiguchi, M. Yamamoto, T. Tsuda, T. Nakamura, M. K. Yamamoto,

427   T. Sato, M. Hagio, and Y. Yabugaki:. Equatorial Atmosphere Radar (EAR):

428   System description and first results. Radio Science, 38(3), 1053, 2003.

429   Gage, K. S., and Green, J. L.: An objective method for the determination of tropopause

430   height from VHF radar observations. Journal of Applied Meteorology, 21(21),

431   1150-1154, 1982.

432   Gage, K. S., and Green, J. L.: Tropopause Detection by Partial Specular Reflection with

433   Very-High-Frequency Radar. Science, 203(4386), 1238-1240, 1979.

434   Gettelman, A., P. Hoor, L. L. Pan, W. J. Randel, M. I. Hegglin, and T. Birner: The

435   extratropical upper troposphere and lower stratosphere, Reviews of Geophysics,

436   49(3), RG3003, doi: 10.1029/2011RG000355, 2011.

437   Hermawan, E., Tsuda, T., and Adachi, T.: MU radar observations of tropopause

438   variations by using clear air echo characteristics. Earth, Planets and Space, 50(4),

439   361-370, 1998.

440   Hall, C.: The radar tropopause above Svalbard 2008–2012: Characteristics at various

441   timescales. Journal of Geophysical Research, 118(6), 2600-2608, 2013a.

442   Hall, C.: The radar tropopause at 78°N, 16°E: Characteristics of diurnal variation.

443   Journal of Geophysical Research, 118(12), 6354-6359, doi:10.1002/jgrd.50560,

444   2013b.

445   Hall, C. M., Röttger, J., Kuyeng, K., Sigernes, F., Claes, S., and Chau, J. L.: Tropopause

446   altitude detection at 78°N, 16°E, 2008: First results of the refurbished SOUSY

447   radar. Radio Science, 44(5), 1-12, doi:10.1029/ 2009RS004144, 2009.

448   Hoinka, K. P.: Statistics of the Global Tropopause Pressure. Monthly Weather Review,

449   126(12), 3303-3325, 1998.

450   Hoskins, B. J., Mcintyre, M. E., and Robertson, A. W.: On the use and significance of

451   isentropic potential vorticity maps. Quarterly Journal of the Royal Meteorological

452   Society, 111(470), 877-946, 2007.

453   Huang, C., Zhang, S. D., Zhou, Q. H., Yi, F., Huang, K., Gong, Y., Zhang, Y., and Gan,

454   Q.: WHU VHF radar observations of the diurnal tide and its variability in the lower

455   atmosphere over Chongyang (114.14° E, 29.53° N), China. Annales Geophysicae,

456   33(7), 865-874, 2015.

457   Hoerling, M. P., Schaack, T. K., and Lenzen, A. J.: Global Objective Tropopause

458   Analysis. Monthly Weather Review, 119(8), 1816-1831, 1991.

459   Liu, Y., Xu, T., and Liu, J.: Characteristics of the seasonal variation of the global

460   tropopause revealed by cosmic/GPS data. Advances in Space Research, 54(11),

461   2274-2285, 2014.

462   May, P. T., Yamamoto, M., Fukao, S., Sato, T., Kato, S., and Tsuda, T.: Wind and

463   reflectivity fields around fronts observed with a VHF radar. Radio Science, 26(5),

464   1245-1249, 1991.

465   Nastrom, G. D., Green, J. L., Gage, K. S., and Peterson, M. R.: Tropopause Folding

466   and the Variability of the Tropopause Height as Seen by the Flatland VHF Radar.

467   Journal of Applied Meteorology, 28(12), 1271-1281, 1989.

468   Nielsen-Gammon, J. W.: A visualization of the global dynamic tropopause. Bulletin of

469   the American Meteorological Society, 82(6), 1151-1168, 2001.

470   Pan, L. L., Randel, W. J., Gary, B. L., Mahoney, M. J., and Hintsa, E. J.: Definitions

471   and sharpness of the extratropical tropopause: A trace gas perspective. Journal of

472   Geophysical Research, 109, D23103, doi:10.1029/2004JD004982, 2004.

473   Pan, L. L., W. J. Randel, J. C. Gille, W. D. Hall, B. Nardi, S. Massie, V. Yudin, R.

474   Khosravi, P. Konopka, and D. Tarasick: Tropospheric intrusions associated with

475   the secondary tropopause, Journal of Geophysical Research, 114, D10302, 2009.

476   Press, W. H., and Rybicki, G. B.: Fast algorithm for spectral analysis of unevenly

477   sampled data. The Astrophysical Journal, 338(1), 277-280, 1989.

478   Ravindrababu, S., Venkat Ratnam, M., Sunilkumar, S. V., Parameswaran, K., and

479   Krishna Murthy, B. V.: Detection of tropopause altitude using Indian MST radar

480   data and comparison with simultaneous radiosonde observations. Journal of

481   Atmospheric and Solar-Terrestrial Physics, 121(6), 679-687, 2014.

482   Randel, W. J., Wu, F., and Gaffen, D. J.: Interannual variability of the tropical

483   tropopause derived from radiosonde data and NCEP reanalyses. Journal of

484   Geophysical Research Atmospheres, 105(D12), 15509-15523, 2000.

485   Randel, W. J., Seidel, D. J., and Pan, L. L.: Observational characteristics of double

486   tropopauses. Journal of Geophysical Research, 112, D07309, 2007.

487   Randel, W. J., and Wu, F.: The Polar Summer Tropopause Inversion Layer. Journal of

488   the Atmospheric Sciences, 67(8), 2572-2581, 2010.

489   Randel, W. J., Wu, F., and Forster, P. M.: The extratropical tropopause inversion layer:

490   Global observations with GPS data, and a radiative forcing mechanism. Journal of

491   the Atmospheric Sciences, 64(12), 4489-4496, 2007.

492   Ramakrishnan, K. P.: Distortion of the tropopause due to meridional movements in the

493   sub-stratosphere. Nature, 132(3346), 932-932, 1933.

494   Roettger, J.: Observations of the polar d-region and the mesosphere with the Eiscat

495   Svalbard radar and the SOUSY Svalbard Radar (scientific paper). Memoirs of

496   National Institute of Polar Research. Special Issue, 54(94), 9-20, 2001.

497   Reed, R. J.: A study of a characteristic tpye of upper-level frontogenesis. Journal of the

498   Atmospheric Sciences, 12(3), 226-237, 1955.

499   Santer, B. D., Wehner, M. F., Wigley, T. M., Sausen, R., Meehl, G. A., Taylor, K. E.,

500   Ammann, C., Arblaster, J., Washington, W. M., Boyle, J. S., and Brüggemann, W.:

501   Contributions of anthropogenic and natural forcing to recent tropopause height

502   changes. Science, 301(5632), 479-483, 2003.

503 Santer, B. D., Sausen, R., Wigley, T. M., Boyle, J. S., Achutarao, K., Doutriaux, C.,

504   Hansen, J. E., Meehl, G. A., Roeckner, E., Ruedy, R., Schmidt, G., and Taylor, K.

505   E.: Behavior of tropopause height and atmospheric temperature in models,

506   reanalyses, and observations: Decadal changes. Journal of Geophysical Research,

507   108(D1), 4002, doi:10.1029/2002JD002258, 2003a.

508 Sausen, R., and Santer, B. D.: Use of Changes in Tropopause Height to Detect Human

509   Influences on Climate. Meteorologische Zeitschrift, 12(3), 131-136, 2003.

510 Schmidt, T., Heise, S., Wickert, J., Beyerle, G., & Reigber, C.: GPS radio occultation

511   with CHAMP and SAC-C: global monitoring of thermal tropopause parameters.

512   Atmospheric Chemistry and Physics, 5(6), 1473-1488, 2005.

513 Seidel, D. J., Ross, R. J., Angell, J. K., and Reid, G. C.: Climatological characteristics

514   of the tropical tropopause as revealed by radiosondes. Journal of Geophysical

515   Research, 106(D8), 7857-7878, 2001.

516 Son, S. W., Tandon, N. F., & Polvani, L. M.: The fine-scale structure of the global

517   tropopause derived from COSMIC GPS radio occultation measurements. Journal

518   of Geophysical Research: Atmospheres, 116(D20), 2011.

519 Sprenger, M., Croci Maspoli, M., and Wernli, H.: Tropopause folds and cross-

520   tropopause exchange: a global investigation based upon ECMWF analyses for the

521   time period March 2000 to February 2001. Journal of Geophysical Research

522   Atmospheres, 108(12), 291-302, 2003.

523 Tian, Y., and Lu, D.: Comparison of Beijing MST Radar and Radiosonde Horizontal

524   Wind Measurements. Advances in Atmospheric Sciences, 34(1), 39-53. doi:

525   10.1007 / s00376-016-6129-4, 2017.

526   Vaughan, G., Howells, A., and Price, J. D.: Use of MST radars to probe the mesoscale

527   structure of the tropopause. Tellus A, 47(5), 759-765, 1995.

528   Wang, C.: Development of the Chinese meridian project. Chinese Journal of Space

529   Science, 30(4), 382–384, 2010.

530   Wilcox L.J., Hoskins B.J., Shine K.P. 2012. A global blended tropopause based on ERA

531   data. Part I: Climatology. Q. J. R. Meteorol. Soc. 138: 561–575.

532   DOI:10.1002/qj.951.

533   Wirth, V.: Thermal versus dynamical tropopause in upper-tropospheric balanced flow

534   anomalies. Quarterly Journal of the Royal Meteorological Society, 126(562), 299-

535   317, 2000.

536   Wirth, V.: Cyclone-anticyclone asymmetry concerning the height of the thermal and the

537   dynamical tropopause. Journal of the Atmospheric Sciences, 58(1), 26-37, 2001.

538   WMO: Definition of the tropopause. WMO Bull., 6, 136, 1957.

539   Yamamoto, M., Oyamatsu, M., Horinouchi, T., Hashiguchi, H., and Fukao, S.: High

540   time resolution determination of the tropical tropopause by the Equatorial

541   Atmosphere Radar. Geophysical Research Letters, 30(21), 2094, 2003.

542   Zängl, G., and Hoinka, K. P.: The tropopause in the polar regions. Journal of Climate,

543   14(2001), 3117-3139, 2001.

544

545 **Table**

Radar parameter	Value
Transmitted frequency	50 MHz
Antenna array	24×24 3-element Yagi
Antenna gain	33 dB
Transmitter peak power	172 kW
Code	16-bit complementary
No. coherent integrations	128 (low mode)/64 (mid mode)
No. FFT points	256
No. spectral average	10
Pulse repetition period	160 (low mode)/320 (mid mode) μs
Half power beam width	3.2^o
Pulse length	1 (low mode)/4 (mid mode) μs
Range resolution	150 (low mode)/600 (mid mode) m
Temporal resolution	30 min
Off-zenith angle	15°

546 **Table 1.** Routine operational parameters in low and middle mode for the Beijing MST

547 radar used in this study.

548
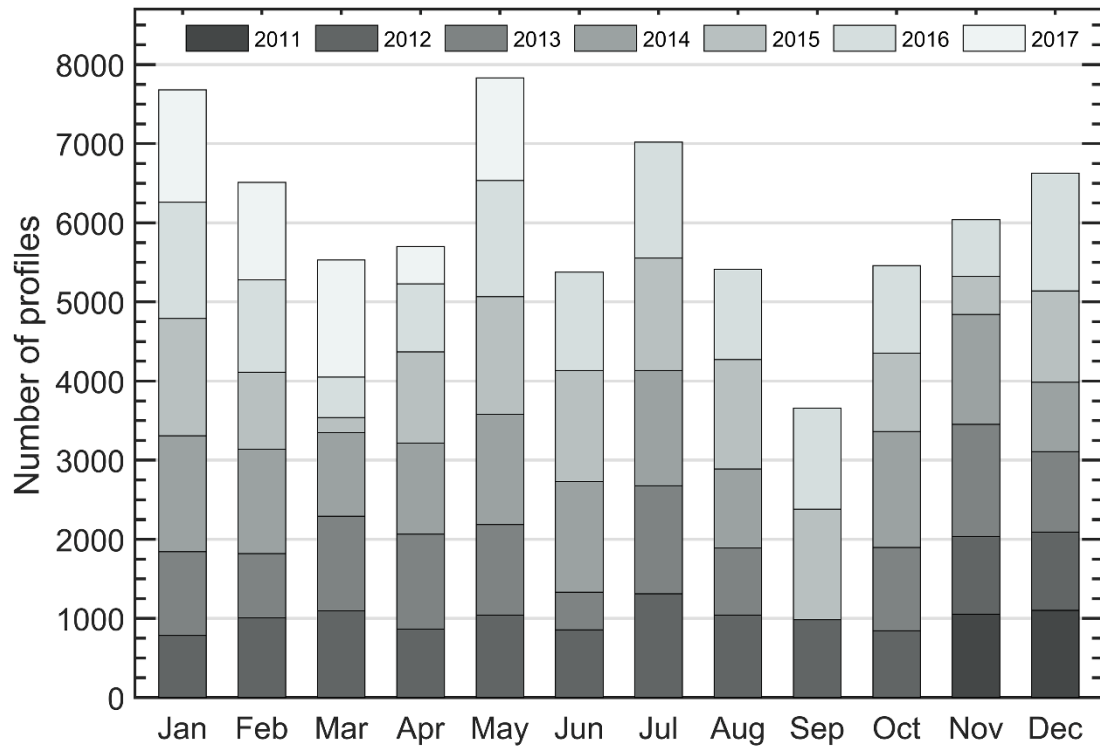
Figures

Figure 1. Distribution of the monthly total number of radar return echo power profiles

that available from vertical beam in low mode, collected for the period November 2011-

May 2017.
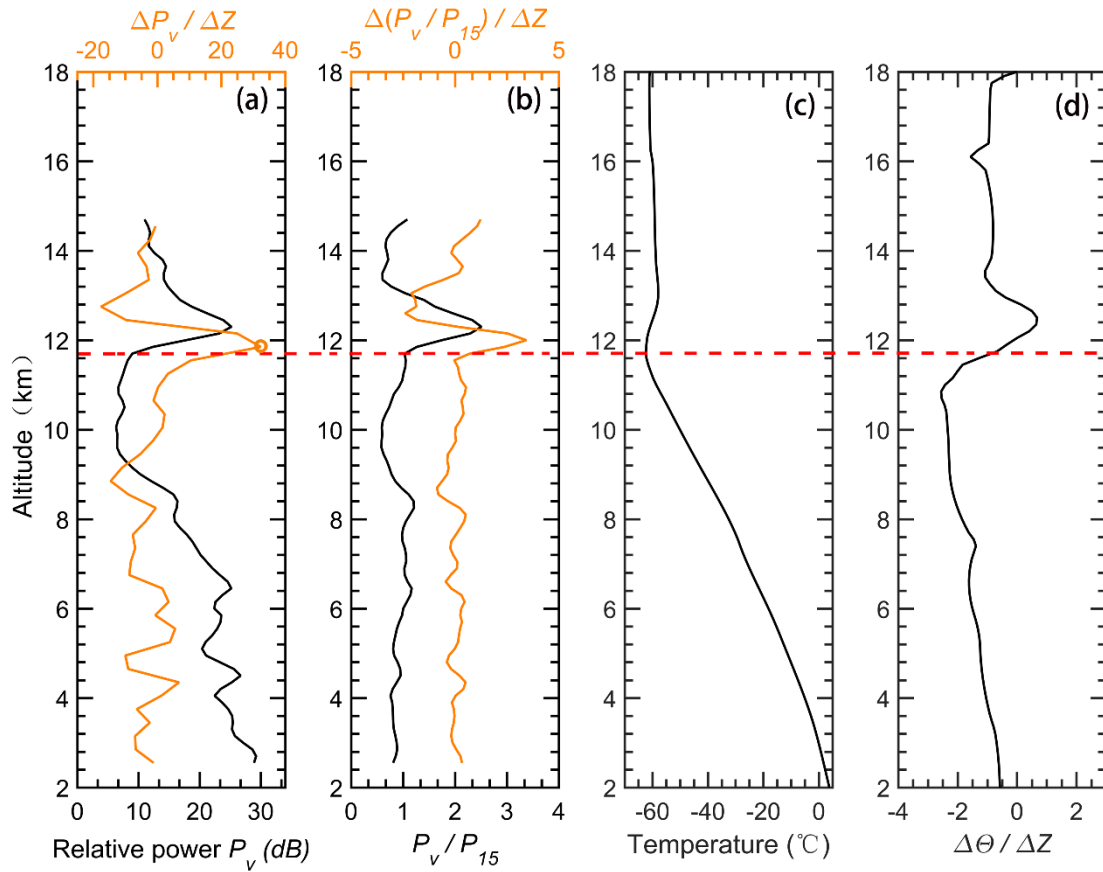
Figure 2. Example vertical profiles of (a) relative radar echo power (black line) along with its gradient variation (orange line), (b) radar aspect sensitivity (black line) along with its gradient variation (orange line), (c) radiosonde temperature and (d) potential temperature gradient on 00 UT 04 November 2011. The horizontal red dashed line marks the LRT height. The orange circle in Fig. 2a denotes the RT height.

562
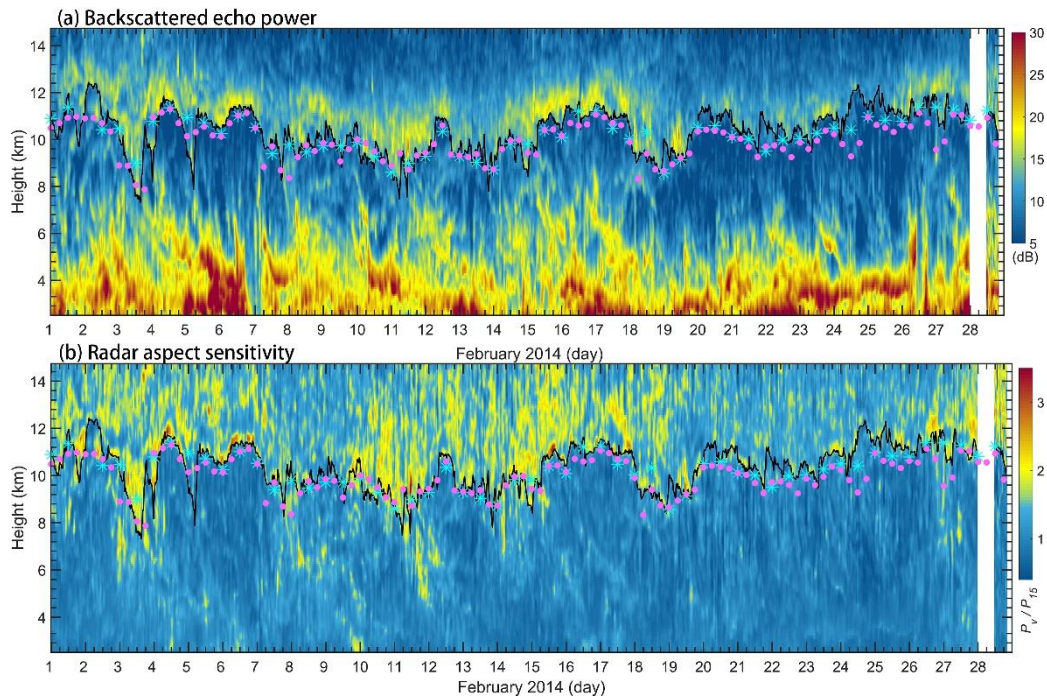
Figure 3. Altitude-time intensity plot of (a) radar backscattered echo power and (b)

radar aspect sensitivity for February 2014. The tropopauses determined based on the

radar echo definition are shown as a black solid curve. The cyan asterisks '*' and pink

dots indicate the location of the LRT derived from simultaneous twice daily radiosonde

data and the PVT from ECMWF ERA-Interim reanalysis, respectively. White stripe

indicates the time frame of radar missing data.
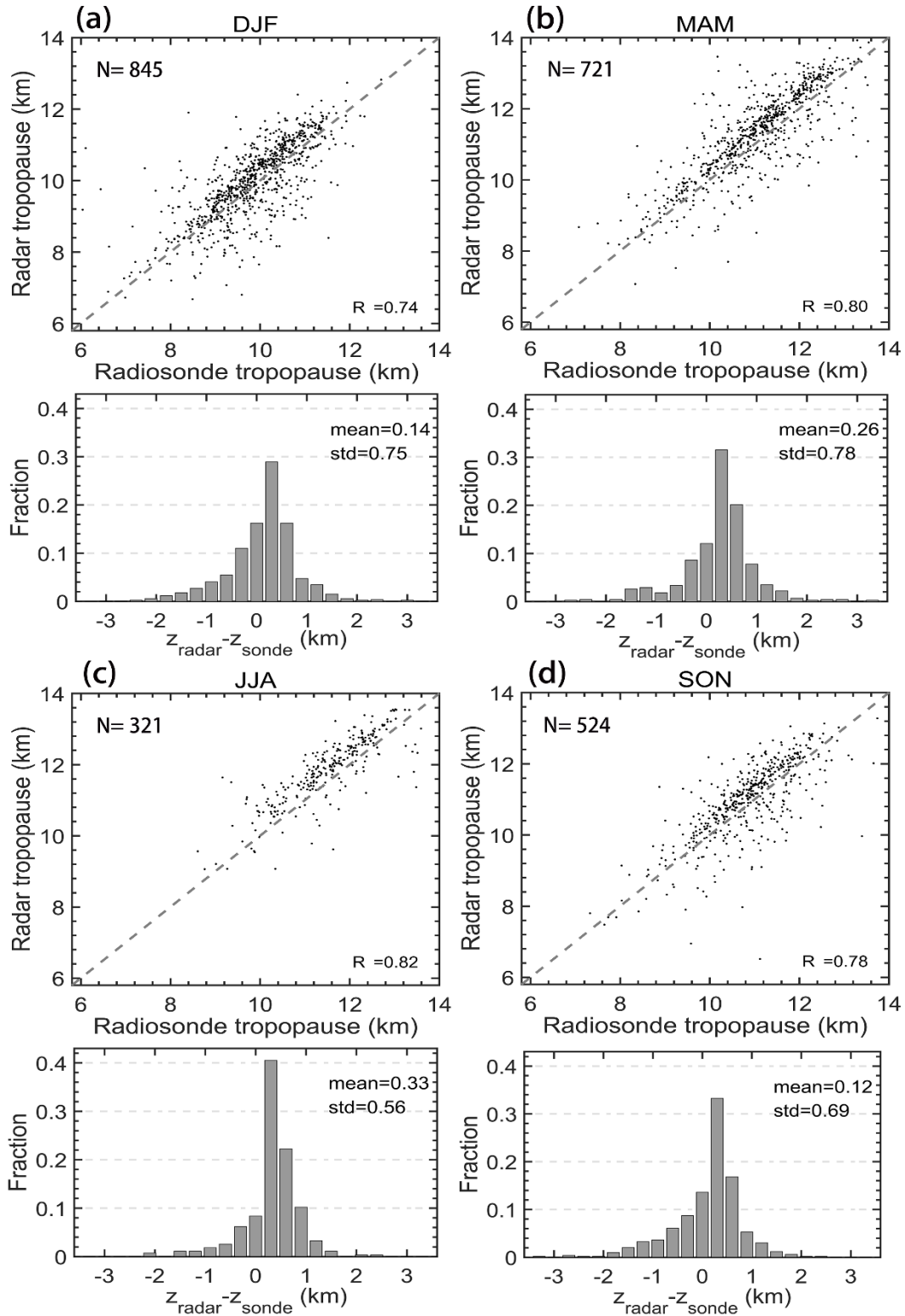
Figure 4. Seasonal scatterplots of the RT versus LRT and histogram distribution of altitude differences between the RT and the LRT, for (a) winter DJF, (b) spring MAM, (c) summer JJA, and (d) autumn SON, during the period November 2011-May 2017.

574   The positive values in the histogram indicate the RT locating at a higher level than the

575   LRT. The grey dashed line shows the 1:1 line. Here, 'N','R^2', 'mean', and 'std' indicate

576   the sample numbers, correlation coefficient, mean difference, and standard deviation of

577   the difference, respectively.

578

579
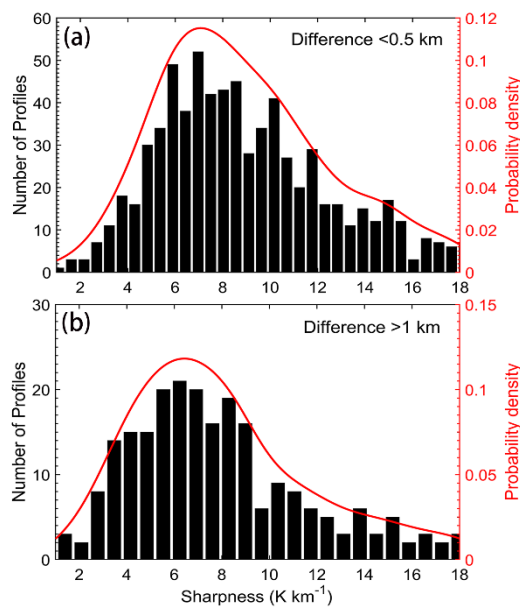
580

581   **Figure 5.** Histogram distribution of the tropopause sharpness for (a) difference <0.5

582   km, and (b) >1 km respectively between the LRT and the RT.

583
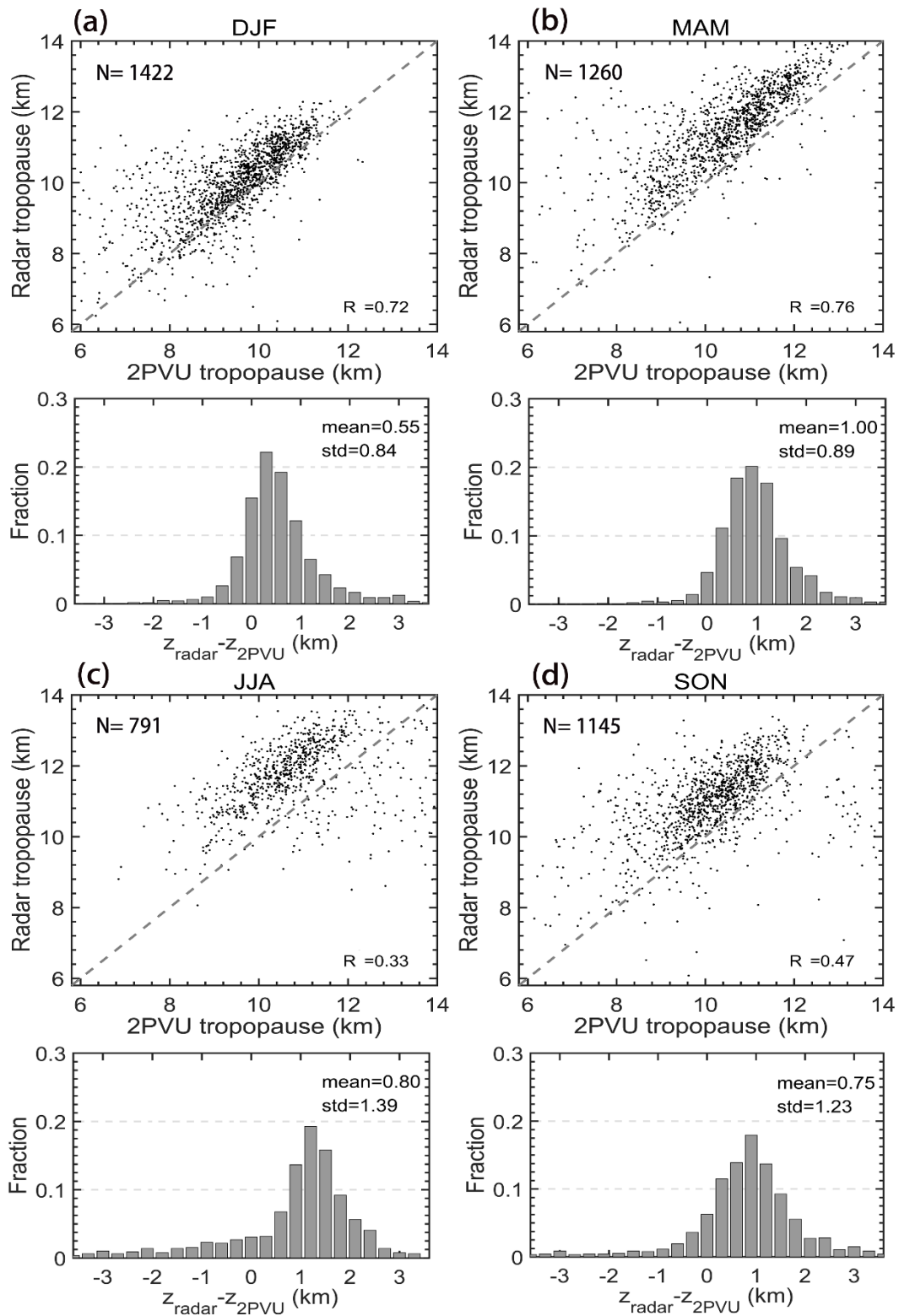
Figure 6. Same as figure 4, but for the comparison between the RT and the PVT.
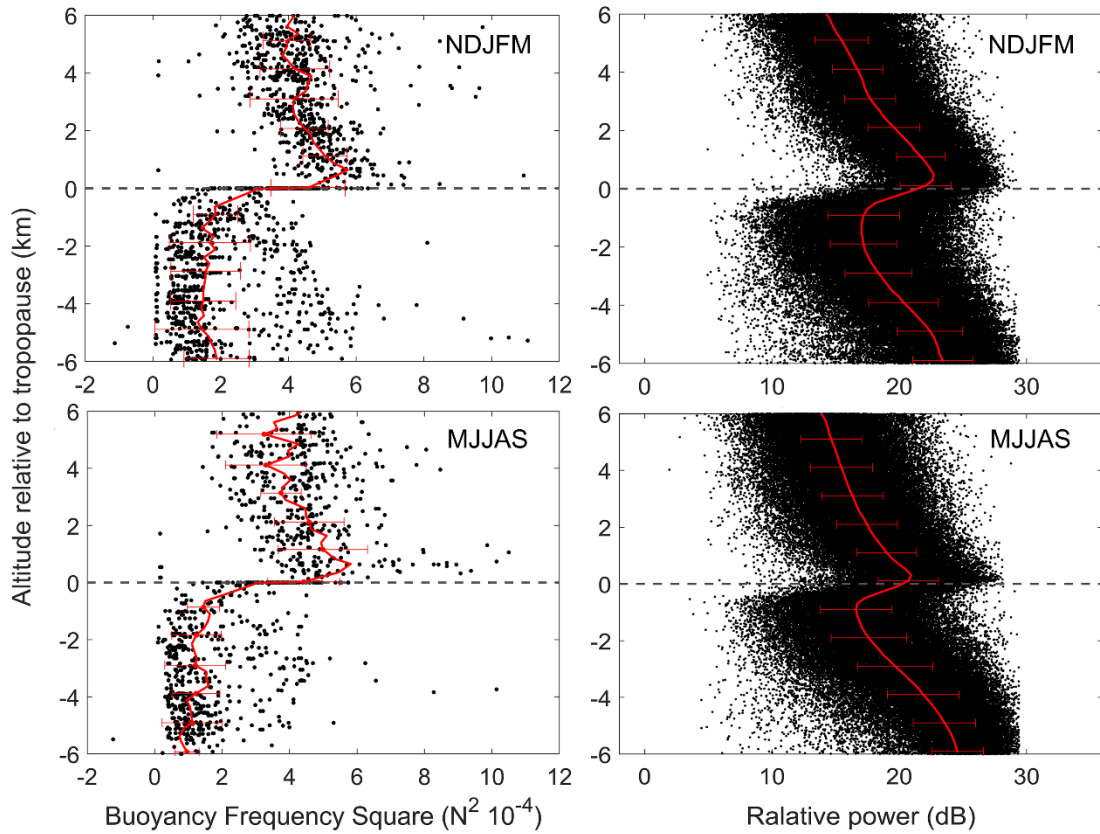
Figure 7. Scatterplots of (left panels) static stability (N^2) and (right panels) radar relative echo power as a function of altitude relative to the LRT (left panels) and RT (right panels) for extended winter (NDJFM) and summer (MJJAS) seasons for two specific years 2012-2013. Red lines in each panel denote the corresponding mean profiles and the error bars indicate the standard deviations.
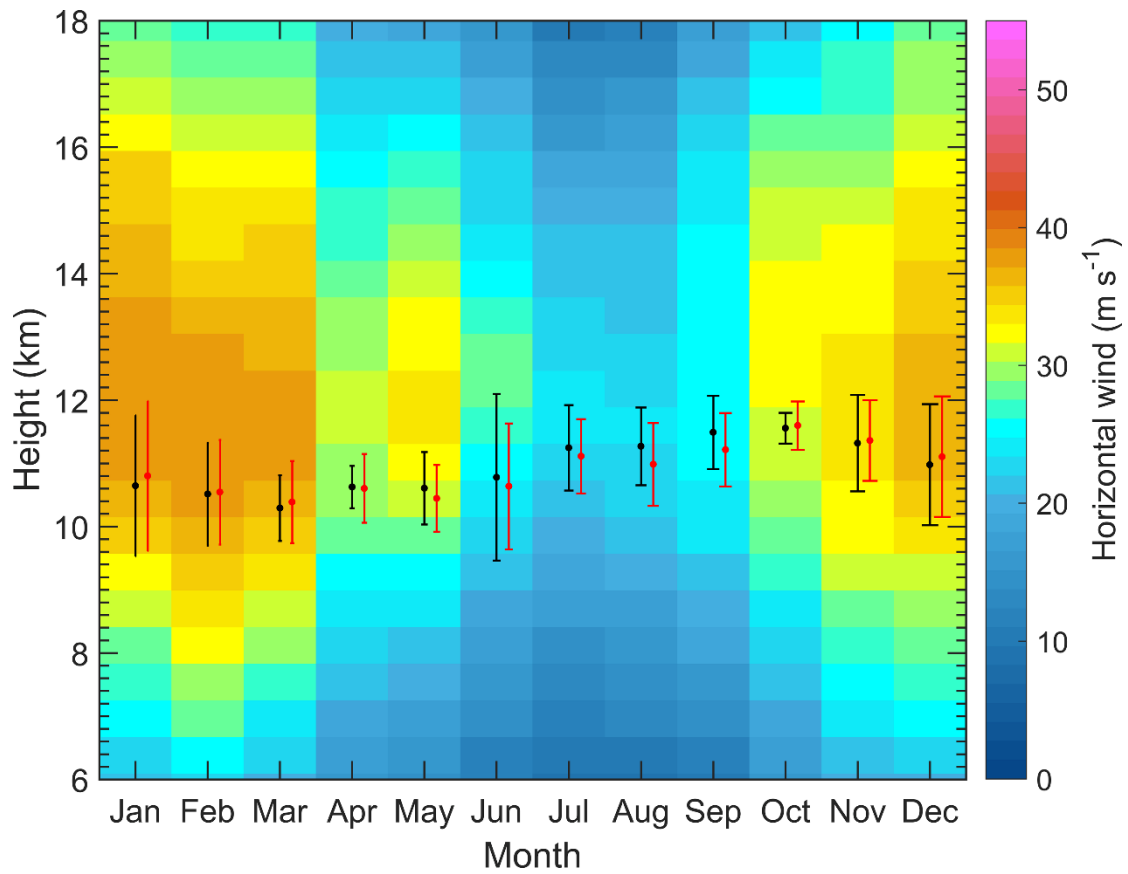
595
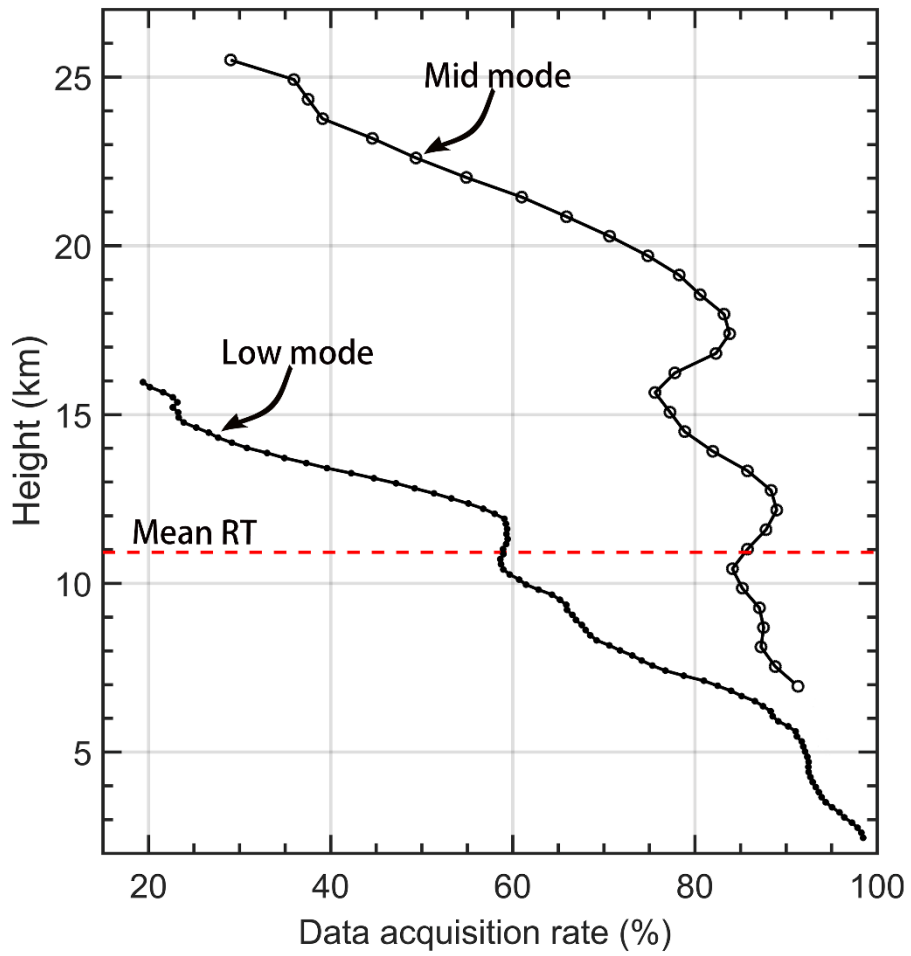
Figure 8. Vertical height profiles of the averaged effective radar wind data acquisition

rate in low mode and middle mode during November 2011-May 2017. The red dashed

line indicates the mean RT height.

599

600

Figure 9. Height-time intensity map of monthly mean horizontal wind speed (shaded, m/s) derived from the middle mode of Beijing MST radar, during November 2011-May 2017. Also shown is the monthly mean height of RT (black dots) and LRT (red dots, offset by +6 days) along with the vertical error bars representing the standard deviations.
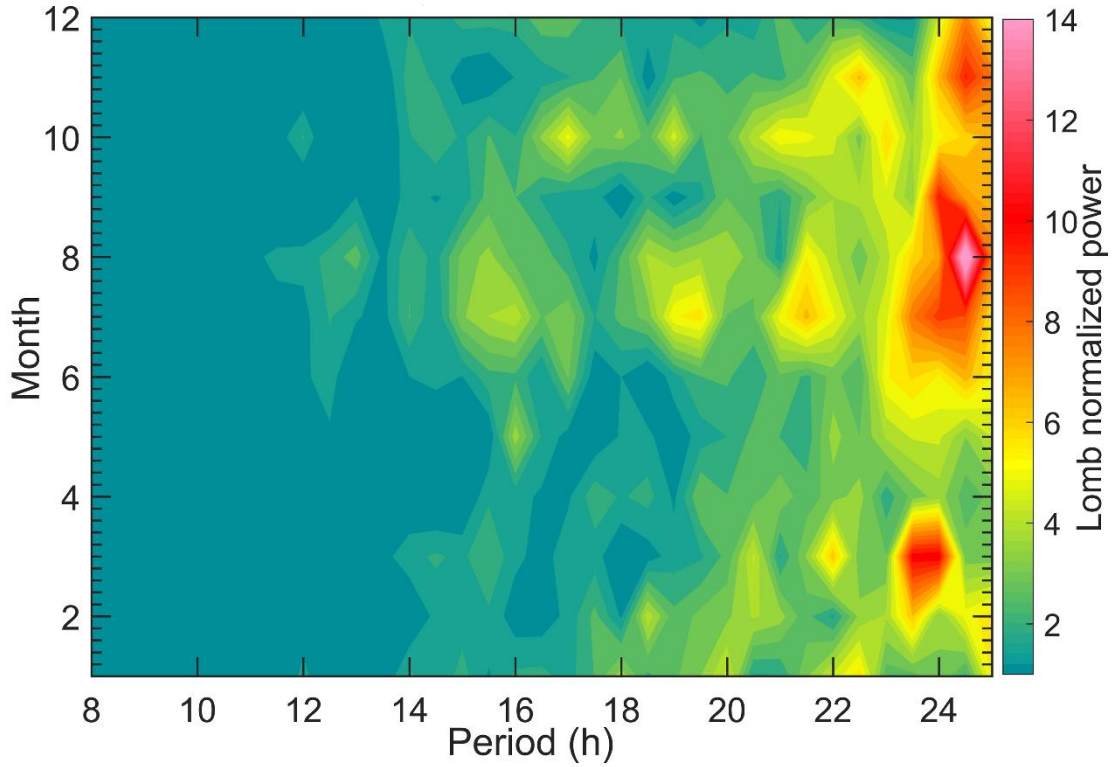
605
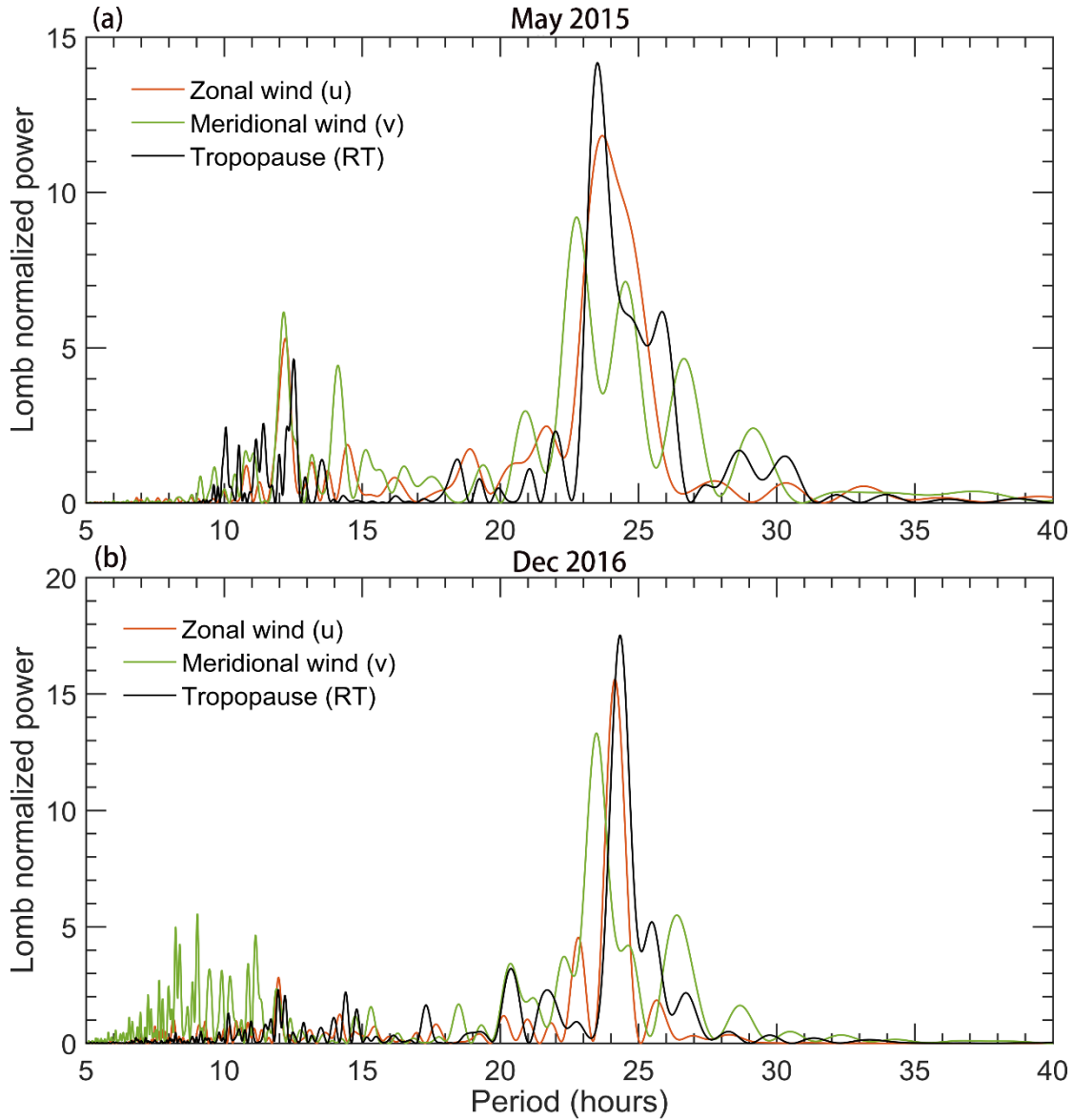
Figure 10. Lomb-Scargle periodograms of the RT height, zonal, and meridional wind oscillations for specific months of (a) May 2015 and (b) December 2016. The zonal and meridional wind for (a) is sampled at 9.85 km and (b) at 11 km.
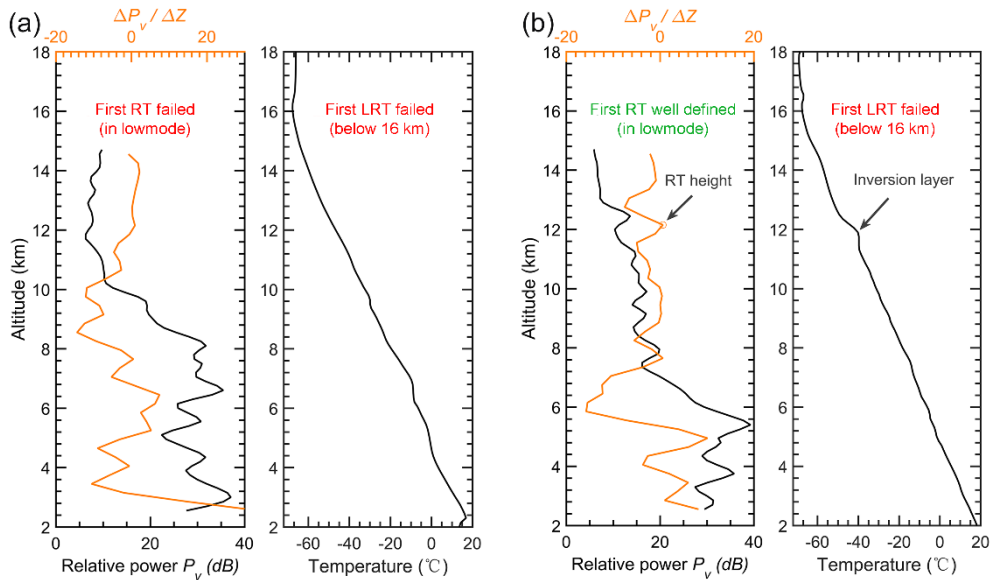
Figure 11. Mean Lomb-Scargle periodograms of RT height as a function of the time of

month during November 2011-May 2017.

Figure 12. Example profiles of radar echo power and radiosonde temperature that (a)

both the RT and LRT definitions fail due to the continuing decrease in temperature on

00 UTC 7 July 2012 and (b) the temperature inversion layer failed to meet the LRT

definition but well defined in RT definition on 12 UTC 02 August 2012. Please note

619   that we only consider the conditions below 16 km.